

GA-A22269

**q-PROFILE MEASUREMENTS
WITH MOTIONAL STARK EFFECT IN DIII-D**

**by
B.W. RICE**

FEBRUARY 1996

GA-A22269

q-PROFILE MEASUREMENTS WITH MOTIONAL STARK EFFECT IN DIII-D

by
B.W. RICE*

This is a preprint of a paper to be presented at the Seventh International Conference on Plasma Physics and Controlled Nuclear Fusion, November 28 through December 1, 1995, Tokai, Japan and to be published in the *Proceedings*.

*Present address: General Atomics, P.O. Box 85608, San Diego, California 92186-9784.

**Work supported by
the U.S. Department of Energy
under Contract Nos. DE-AC03-89ER51114
and W-7405-ENG-48**

**GA PROJECT 3466
FEBRUARY 1996**

ABSTRACT

Motional Stark Effect (MSE) has emerged as the most reliable technique for the measurement of q profiles in tokamaks equipped with neutral beams. On DIII-D, two separate 8-channel MSE instruments are utilized, giving 16 radial measurements. The viewing geometry for each instrument is designed to optimize radial resolution ($1.5 \text{ cm} < \delta R < 6 \text{ cm}$) over the measurement range. Dual-frequency polarization modulators combined with lock-in detection provides maximum signal-to-noise with a time response of $\sim 1 \text{ ms}$. Special consideration has gone into the design of the collection optics to minimize undesirable polarization effects on reflectors and Faraday rotation in lenses. Examples of data from negative central magnetic shear, VH-mode, and sawtooth discharges highlight the capabilities of the DIII-D MSE diagnostic.

1. INTRODUCTION

The recent development of plasma diagnostics to measure the safety factor profile $q(r)$, has led to a rapid advance in the understanding of plasma stability and confinement in tokamaks. Modeling MHD instabilities such as sawteeth or the β limiting $n=1$ kink, depends critically on a detailed knowledge of the q profile. Recent experiments with current ramps and negative central magnetic shear indicate that details of the q profile also affects plasma confinement. Thus, accurate measurements of the q profile enables us to optimize plasma stability and confinement to improve tokamak performance.

Motional Stark Effect (MSE) has emerged as the most successful technique for measurement of the q profile in tokamaks with neutral beams. MSE provides a measurement of the local magnetic field pitch angle B_{pol}/B_T . When used as input to an equilibrium reconstruction code, MSE measurements provide a simple and direct constraint on the q profile.

MSE was first demonstrated on PBX-M (Levinton [1]), and a single channel scannable system was installed soon thereafter on DIII-D (Wroblewski [2].) The DIII-D instrument was upgraded to 8 channels in 1992 (Wroblewski [3]), and eventually to 16 channels in 1994 (Rice [4]). In this paper, we describe the basic MSE design constraints and the implementation of the instrument on DIII-D. Calibration methods are discussed in Section 3 and equilibrium reconstruction in Section 4. Finally, q profile data will be presented in Section 5 for several types of discharges where MSE measurements have made a large impact on the DIII-D experimental program: these include sawteeth, VH-mode, and negative central magnetic shear.

2. MSE INSTRUMENT DESIGN

A. Measurement geometry

The MSE measurement relies upon the splitting of the high-energy (80 keV) neutral beam Balmer- α line (D_α) into orthogonally polarized components (σ , π) as a result of the strong motional $\mathbf{E} = \mathbf{v} \times \mathbf{B}$ electric field produced in the rest frame of the neutral deuterium atoms traveling with velocity \mathbf{v} . When viewed in a direction perpendicular to \mathbf{E} , the Stark split σ and π components are polarized perpendicular and parallel to the direction of the electric field respectively. By measuring the polarization of the central σ line, the local pitch angle of the magnetic field B_{pol}/B_T can be determined.

In order to achieve good signal-to-noise and optimum radial resolution, the viewing geometry for MSE must be considered carefully. On DIII-D, in order to optimize radial resolution, we have installed two separate instruments with different viewing geometries as shown in Fig. 1. The central MSE instrument views the Doppler blue-shifted Stark spectrum, while the edge MSE instrument views the red-shifted spectrum. The positions of the key spectra lines for typical chords in the central and edge MSE systems are simulated in Figs. 2(a) and 2(b). The MSE measurement relies on determining the polarization of the full-energy σ component. In order to adequately resolve the local magnetic field pitch angle from this measurement, three criteria must be satisfied for each MSE channel: (1) the induced $\mathbf{v} \times \mathbf{B}$ electric field must be large enough to provide sufficient separation between the σ and π lines; (2) the angle between the optics line of sight and \mathbf{v} ($\Omega + \alpha$ in Fig. 1) must be sufficient to give a large enough Doppler shift to clearly separate the full energy σ peak from thermal D_α , the 1/2 and 1/3 beam energy D_α components, and any background impurity lines which may be present; (3) the optical line of sight must be nearly tangent to the toroidal field for optimum radial resolution.

As seen in Fig. 2, the Stark spectrum is comprised of nine components which have appreciable intensity (shown by the vertical lines). The wavelength splitting between adjacent components is given by $\Delta\lambda = 2.7574 \times 10^{-7} E \text{ \AA}$. For 80 keV deuterium beam injection at 2.1 T, the splitting is about 1.2 \AA . Beam divergence is 0.6° full width on DIII-D, corresponding to a line broadening of $\sim 0.3 \text{ \AA}$. At full field of 2.1 T on DIII-D, the

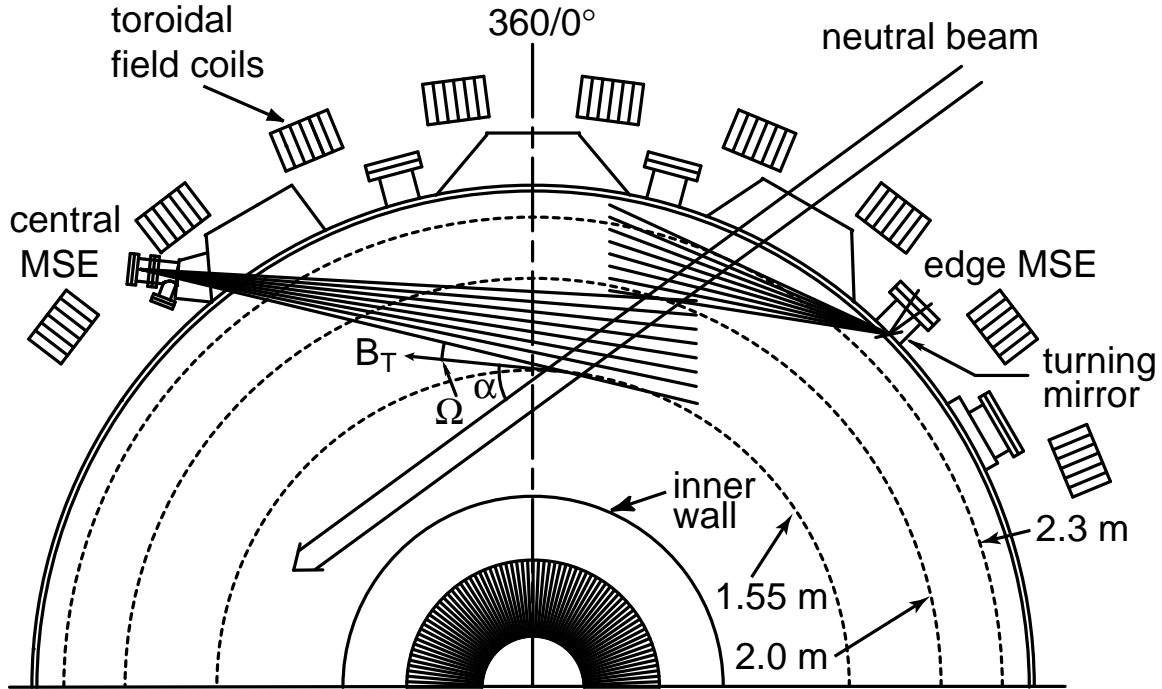


FIG. 1. MSE viewing geometry on DIII-D. Typical locations for the magnetic axis and outer separatrix are 1.75 m and 2.3 m respectively.

separation between the σ and π manifolds is adequate. At fields of <1 T, however, there is significant overlap of the σ and π spectra, which leads to higher noise and uncertainty in the MSE measurements.

The Doppler shift is given by $\delta\lambda = \lambda_{\alpha} v_b/c \cos(\Omega+\alpha)$, which determines the shift away from the thermal D_{α} line (6561 \AA), and the separation between the 1/3, 1/2 and full energy components. Perhaps the most serious constraint is avoidance of the CII impurity lines (at 6578 and 6583 \AA) in the red-shifted part of the spectrum shown in Fig. 2(b). This restricts the viewing angle relative to the beam direction to angles $\Omega+\alpha < 60^\circ$.

The neutral beam has finite width (14 cm e -folding full width), so adequate radial resolution requires a nearly tangential viewing angle relative to the toroidal field direction. Radial resolution is given approximately by $\delta R = (d \sin \alpha + w \sin \Omega)/\sin(\Omega+\alpha)$ where d is the optical spot size and w is the beam width. With a single view, it is difficult to obtain adequate resolution over a large radial extent of the plasma. On DIII-D, we utilize two systems to optimize the radial resolution as shown in Fig. 1. The central MSE system has good resolution in the core ~ 2 cm, while the edge system has resolution of <2 cm near the separatrix. At mid radius where the two instruments overlap and the viewing angle deviates more from tangential, the resolution is ~ 6 cm.

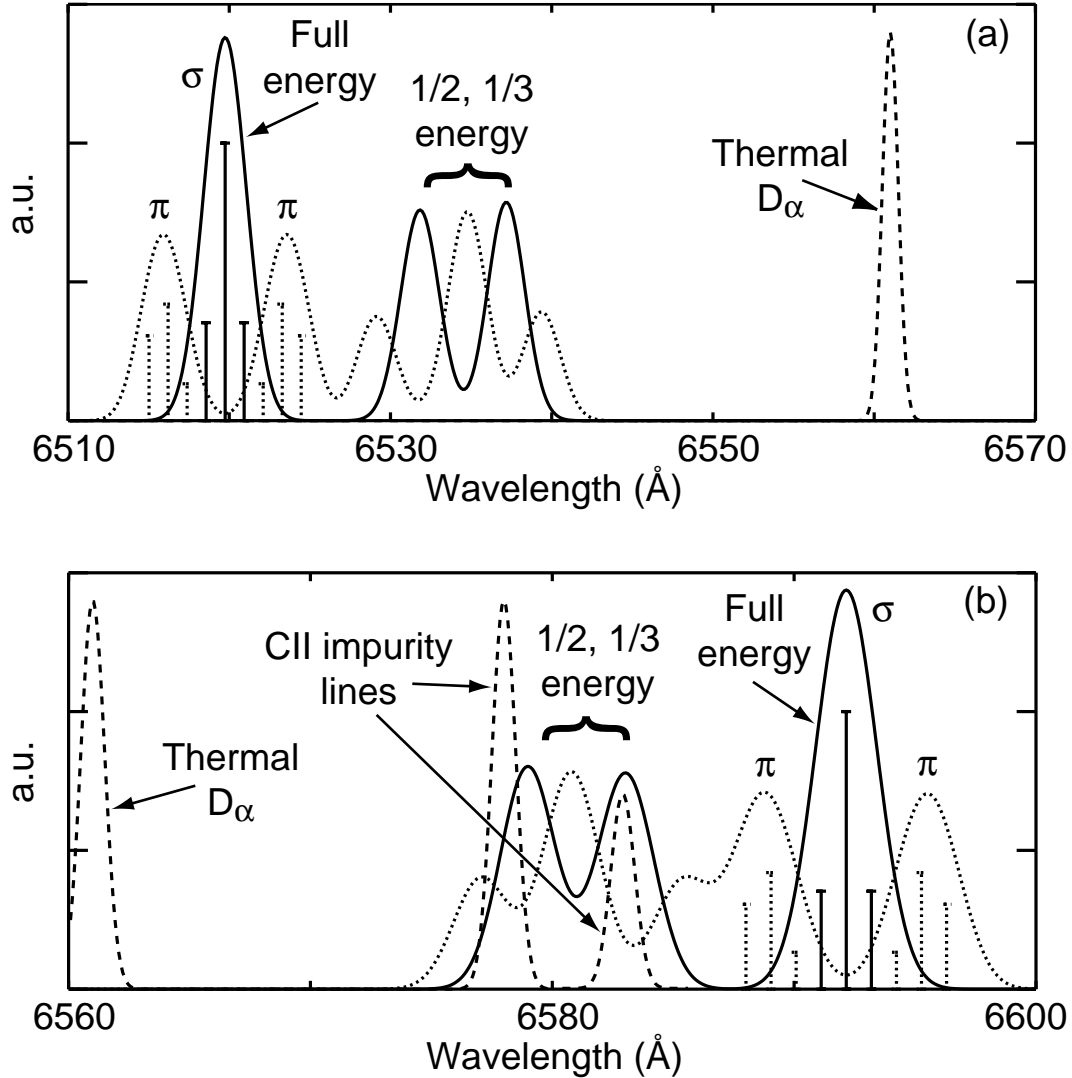


FIG. 2. Position of MSE spectral lines for (a) central MSE blue-shifted spectrum at $R = 1.68$ m, (b) edge MSE red-shifted spectrum at $R = 2.24$ m. Solid lines represent σ components and dotted lines represent π components. (linewidth of 1.5\AA and amplitudes of CII, 1/2, 1/3 components are arbitrary).

The relationship between the measured polarization angle (γ) of the σ component and the magnetic field components (Wroblewski [3]) is given approximately by $\tan\gamma \approx B_z \cos(\alpha + \Omega) / (B_T \sin \alpha)$ where B_z is the vertical field at the midplane.

B. Optics design

An overview of the edge MSE optical system is shown in Fig. 3. Light is collected using a reflector and three lenses. The lenses focus rays through two photoelastic modulators

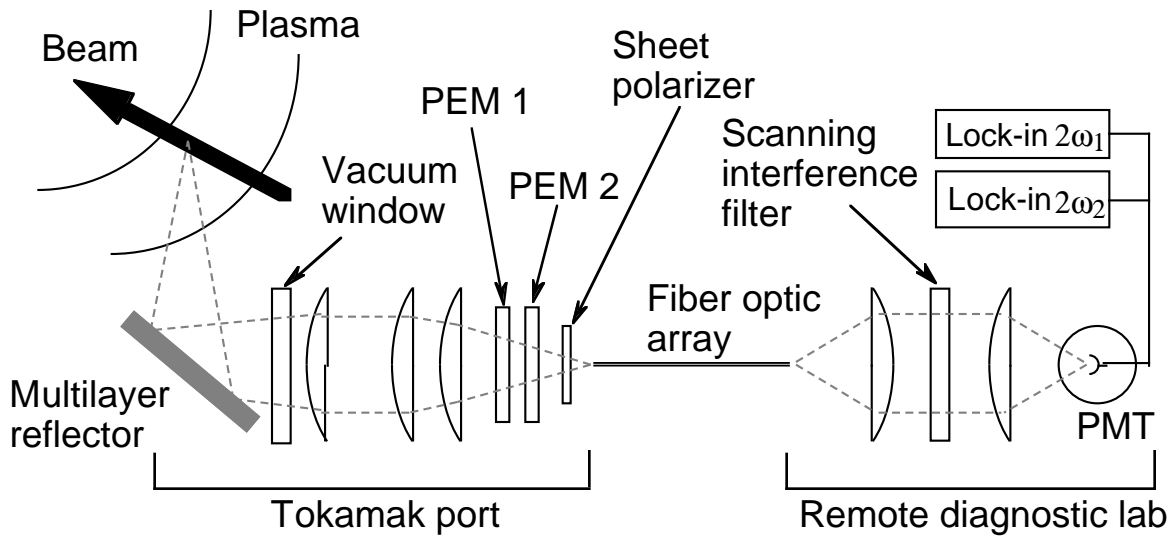


FIG. 3. Overview of MSE collection optics and polarization analyzer.

(PEM), a sheet polarizer, and into an array of six vertically stacked 1 mm diameter fiber optics (six fibers for each channel). The lens combination has a magnification of ~ 10 , which transforms the fiber array into a spot about 1 cm wide and 7 cm high in the plasma, giving good radial resolution. The lenses are located in a strong magnetic field, which causes Faraday rotation of the incoming polarization in ordinary optical glass. To avoid this effect, lenses are constructed out of a near-zero Verdet constant glass SFL6 manufactured by Schott. Although the 1 cm thick vacuum window is still constructed from fused silica, the Faraday rotation effects have been reduced to a $\sim 1^\circ$ level.

The reflector adds a significant complication to the edge MSE design. Ordinary metallic reflectors will reflect orthogonal s and p polarizations with different amplitudes, inducing an effective polarization rotation. On DIII-D we utilize a custom designed multilayer dielectric coated reflector (OCLI [5]), consisting of alternating layers of fused silica and tantalum pentoxide deposited on a fused silica substrate. The surface is durable and vacuum compatible, and the fused silica substrate offers good stability during thermal cycling (vacuum vessel baking reaches 300°C on DIII-D). Design calculations show that the difference in p to s reflectivity is less than 1% over the entire range of angles, while the phase shift is less than 15 degrees for angles of incidence between 48 - 68° .

Returning to Fig. 3, the fiber optic array transmits the collected light from the tokamak port to a remote temperature controlled diagnostic laboratory. Here the light is collimated and passed through a 3 \AA interference filter tuned to the Doppler shift of the neutral beam

D_α line. Fine tuning is accomplished by rotating the filter through small angles using a motorized rotation stage. Following the filter, light is directed onto a Hamamatsu R636 photomultiplier tube. Two lock-in amplifiers then detect the second harmonic of each PEM frequency, which are approximately proportional to the sine and cosine of the polarization pitch angle γ .

The central MSE optics design is similar to that shown in Fig. 3 except, because of the port geometry, there is no need for a reflector. Another difference is that a Wollaston prism is used in place of the sheet polarizer shown in Fig. 3, allowing both polarizations to be collected (two 1×3 fiber bundles, giving six fibers per channel). In the diagnostic room, two photomultipliers are used, one for each polarization, and the signals are then differenced to effectively double the signal level (Wroblewski [3]).

C. Modulation technique

Photoelastic modulators (PEMs) are used to determine the polarization properties of collected light with maximum signal-to-noise. The two PEMs shown in Fig. 3, act as waveplates with retardation oscillations varying between $-\lambda/2$ to $\lambda/2$, where λ is the wavelength. The modulators consist of large octagonal fused silica plates driven at their resonant frequency by a piezoelectric transducer. The induced birefringence causes a modulation of the wave polarization at two different frequencies ω_1 , ω_2 (20 kHz and 23 kHz). The PEMs are followed by a linear polarizer which converts the polarization modulation into intensity modulation. The axes of the modulators are oriented at $+22.5^\circ$ and -22.5° relative to the linear polarizer. The polarization tilt angle is obtained from the simple ratio $\tan 2\gamma = S_1/S_2$ where S_1 , S_2 are the amplitudes of the 2nd harmonic of each PEM frequency.

3. MSE CALIBRATION

Instrument calibration as a function of input polarization angle is accomplished using an integrating sphere light source with a rotatable polarizer mounted on the aperture. The light source is placed inside the DIII-D vacuum vessel and, by backlighting the fiber optics, is aligned with a given channel. The ratio of 2ω lock-in amplifier voltages, S_1/S_2 , is then plotted as a function of polarizer angle as shown in Fig. 4(a). These data are fitted with a three parameter function $S_1/S_2 = c_1 \tan(c_3 2\gamma + c_2)$ where γ is the polarizer angle and c_1, c_2, c_3 are the free parameters.

The next calibration step is to adjust the offset angle (c_2 above). There are two effects to consider: first is simply the difference in zero degree reference between the vacuum toroidal field direction and the polarizer used to produce Fig. 4(a); second is the change in offset angle with B_T due to the Faraday effect in the optics. This offset angle is modeled as $\delta\gamma = b_1 + b_2 B_T$, where b_2 represents the correction due to the Faraday rotation effect in the optics. The coefficients b_1, b_2 are determined by injecting 50 ms neutral beam pulses into a 0.5 mTorr background gas (either D₂ or He) and scanning the toroidal field. Typical results from this calibration are shown in Fig. 4(b), for the original MSE system with BK7 optics, and the upgraded MSE system with SFL6 optical glass and the insertable polarizer. The dramatic reduction in the Faraday rotation effect is evident. This is especially important because Faraday rotation corrections due to the weaker poloidal field can be neglected with the new optics.

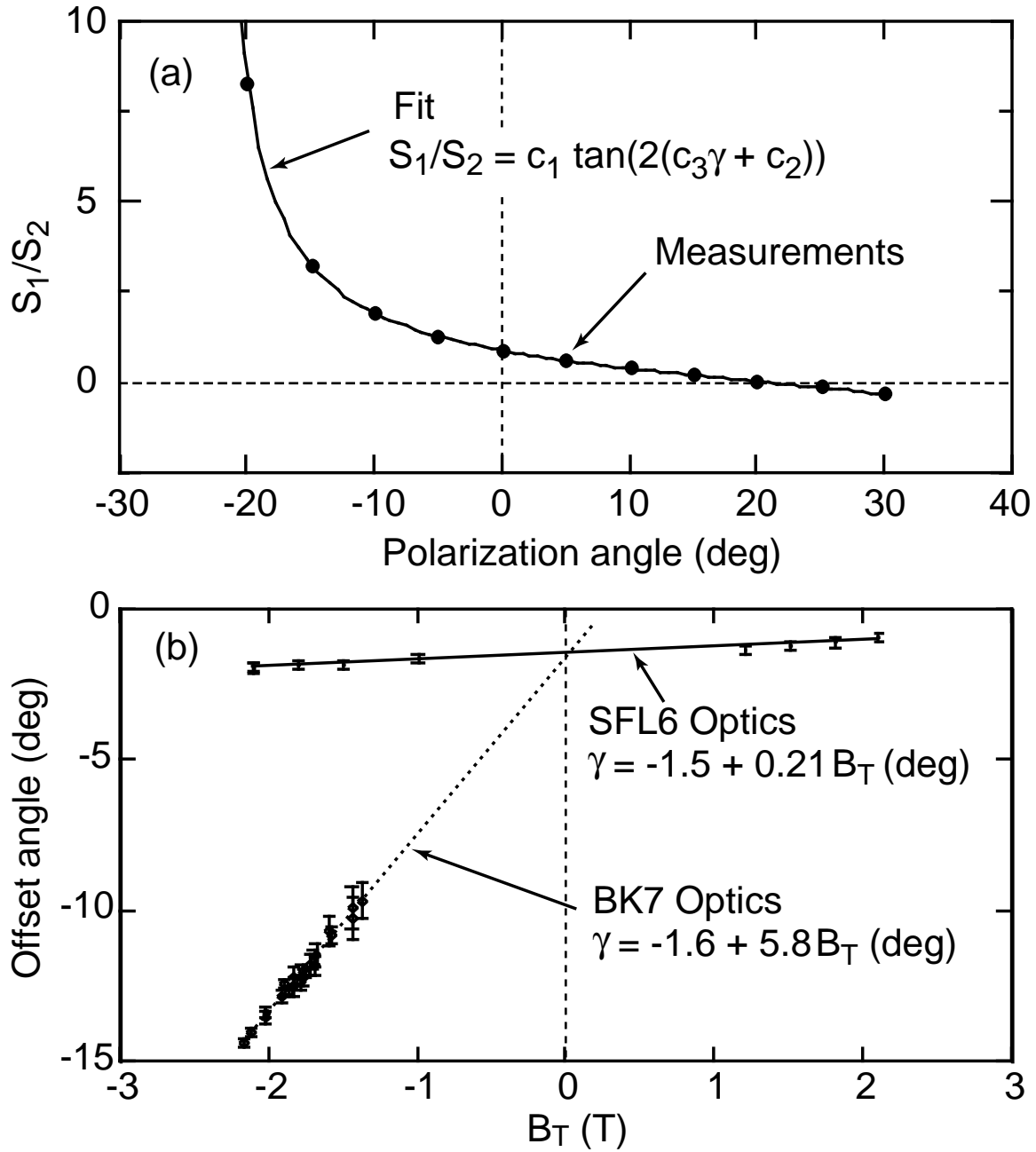


FIG. 4. (a) Polarimeter calibration curve, obtained using an integrating sphere light source and a rotating polarizer (typical plasma pitch angles are < 20 deg; (b) comparison of offset angle vs. B_T for the original BK7 optics (dashed) with large Faraday rotation and the new low Verdet constant glass SFL6 (solid).

4. EQUILIBRIUM RECONSTRUCTION

On DIII-D, equilibrium reconstruction is performed using the EFIT code (Lao [6]) which utilizes all the available equilibrium measurements including magnetic probes, flux loops, Rogowski coils, diamagnetic loops, MSE data, and, optionally, pressure data. EFIT solves the Grad-Shafranov equation $\Delta^* \psi = -\mu_0 R J_T$ while minimizing χ^2 for all the available measurements. The current density J_T is expressed in terms of the flux functions $P'(\psi)$ and $FF'(\psi)$ through $J_T = R P'(\psi) + \mu_0 / (4 \pi^2 R) FF'(\psi)$ where P is the plasma pressure and $F = RB_T$. The free functions $P'(\psi)$ and $FF'(\psi)$ can be parametrized in terms of polynomial or spline basis functions. The spline forms were added recently to fit profiles which exhibit more structure, such as VH-modes with large edge current density or negative central magnetic shear discharges which have a strongly inverted q profile. A single time-slice EFIT reconstruction can usually be performed in <15 s on standard UNIX workstations, which allows 20–50 time slices to be analyzed between discharges on DIII-D (10–15 min).

5. q PROFILE MEASUREMENT RESULTS

The reliable and routine operation of MSE has made a large impact on the DIII-D experimental program over the past few years. In this section, we present MSE data which highlights some of the more interesting results and demonstrates the capability of the instrument.

A. *Sawteeth*

The sawtooth instability, which is observed on all tokamaks, is still not well understood, despite the recent progress in $q(r)$ profile measurements. Many tokamaks have reported q_0 values in the range of 0.7–0.9 during sawteeth, remaining <1 throughout the sawtooth period. DIII-D is perhaps unique in that we generally observe $q_0 \sim 1$ during sawteeth, typically ~ 0.95 before a sawtooth crash and ~ 1.05 after a sawtooth crash (Wroblewski [7]). There are some cases with low q_{95} where q_0 values as low as 0.85–0.9 are observed, but this does not occur frequently.

A typical H-mode discharge with sawteeth is shown in Fig. 5. In Fig. 5(a), the MSE data and corresponding EFIT reconstruction are shown for a timeslice just before a sawtooth crash. The MSE pitch angle measurements have been transformed to B_z measurements for this plot. The magnetic probe data at the wall is also shown. The q profiles before the crash ($q_0 = 0.97$) and after the crash ($q_0 = 1.05$) are shown in Fig. 5(b). The temporal evolution of q_0 is shown in Fig. 5(c), both from EFIT reconstructions (dotted) and from our real-time q_0 algorithm (solid line) which is used by the plasma control system on DIII-D (Ferron [8]). The real-time algorithm calculates q_0 from the relation $q_0 = \kappa_0/R_0/(d\gamma_t/dR)_0$ where $\gamma_t \equiv [\sin \alpha/\cos(\alpha + \Omega)] \tan \gamma$ and $(d\gamma_t/dR)_0$ refers to the slope of this quantity near the magnetic axis. Using an estimate for the elongation on axis, κ_0 , from EFIT, this provides a fast and accurate method for obtaining q_0 with good time resolution. As seen in Fig. 8(c) the agreement with EFIT is quite good. The absolute uncertainty in q_0 is ± 0.06 , determined by an analysis of the uncertainty in the slope of B_z at the magnetic axis in Fig. 5(a)

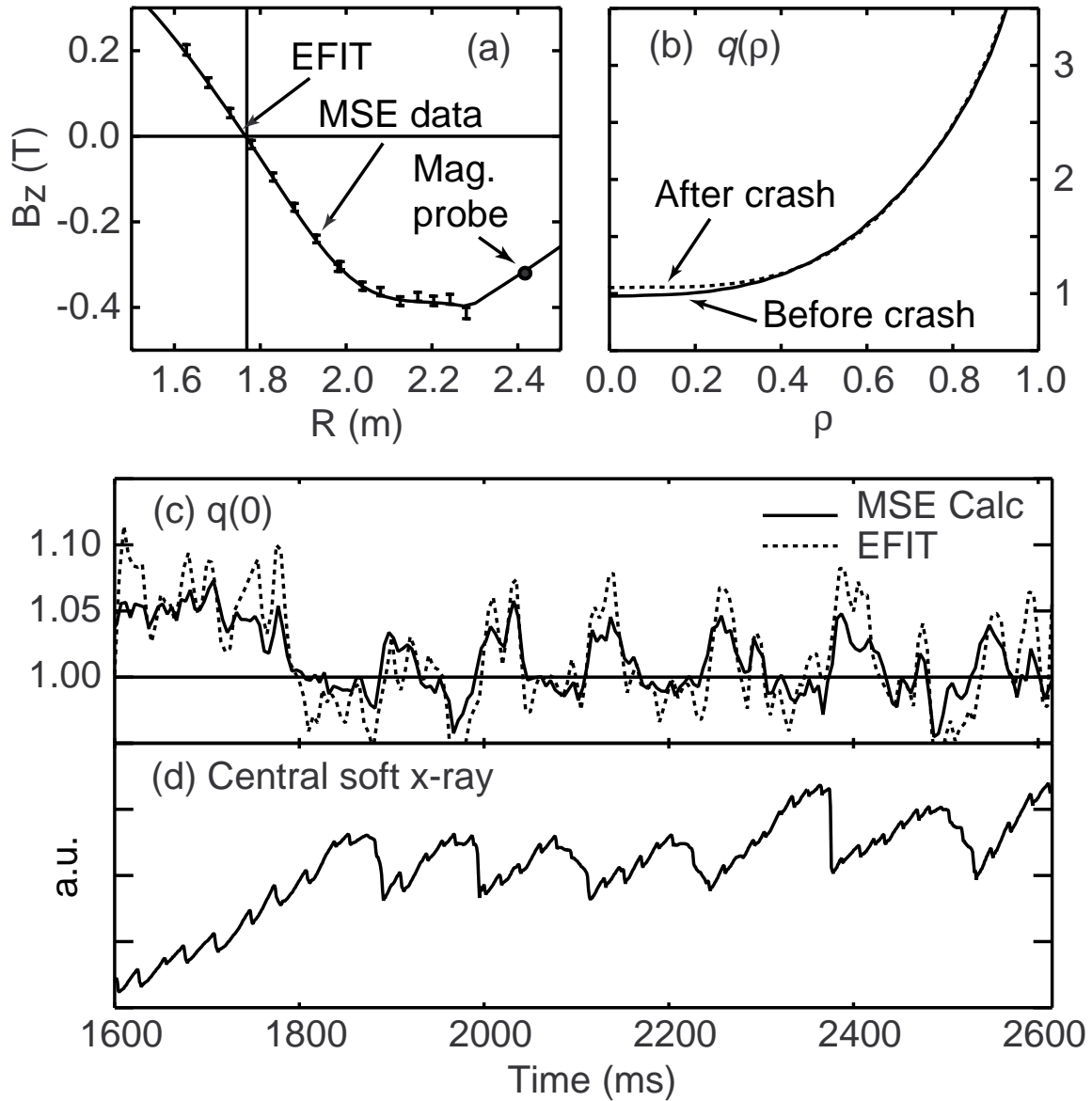


FIG. 5. Sawtooth discharge. (a) MSE measurements of B_z and equilibrium reconstruction (solid curve) just before a sawtooth crash; (b) q profile before crash (solid, $q_0 = 0.97$) and after crash (dotted, $q_0 = 1.05$); (c) q_0 time evolution from EFIT (dotted) and direct from MSE data (solid) with $\kappa_0 = 1.35$; (d) central soft x-ray emission.

B. VH -mode profile evolution

VH -mode discharges have the highest performance on DIII-D in terms of beta and confinement times (Lazarus [9]). The temporal evolution of the q profile plays an important role in the confinement and stability of these discharges. In Fig. 6 we show the time history of q_0 and β during the high performance VH -mode phase. One characteristic of the

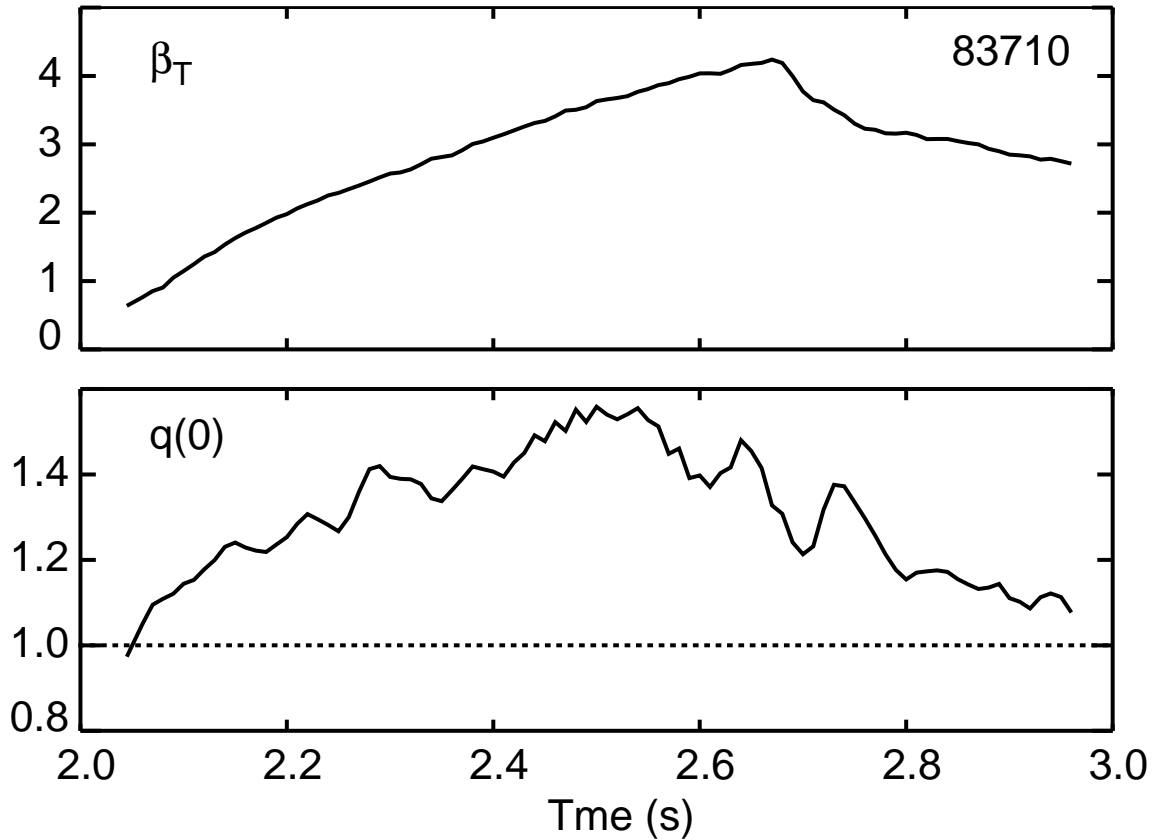


FIG. 6. Time evolution of q_0 and B_T for a standard VH-mode discharge (83710). The ELM-free period extends from 2000–2750 ms and $P_{\text{NBI}} = 8.7$ MW.

VH-mode is the rapid rise in q_0 to >1 , which follows the start of beam injection. This higher value of q_0 provides both Mercier stability and access to the second stability regime for ballooning modes in the core (Lazarus [9]). The evolution of the measured B_z profile and EFIT reconstructed J and q profiles is shown in Fig. 7. The first time slice at 2070 ms, represents the L-mode time prior to the H-mode transition. Note the smooth current density profile, q_0 near unity, and lack of any edge current. The next time slice is 300 ms after the H-mode transition, and shows two dramatic changes. First, q_0 has increased, and second, localized edge current has begun to develop due to bootstrap current driven by the steep edge pressure gradient. The perturbation of the edge poloidal field due to the edge current is clearly seen in the outermost MSE points. In the final time slice at 2670 ms, the edge current has continued to increase and broaden. Shortly after this time the discharge suffers a β collapse triggered by a low- n mode localized near the edge. Control of the edge pressure gradient and resulting edge bootstrap current is an ongoing effort at DIII-D to extend the VH-mode period.

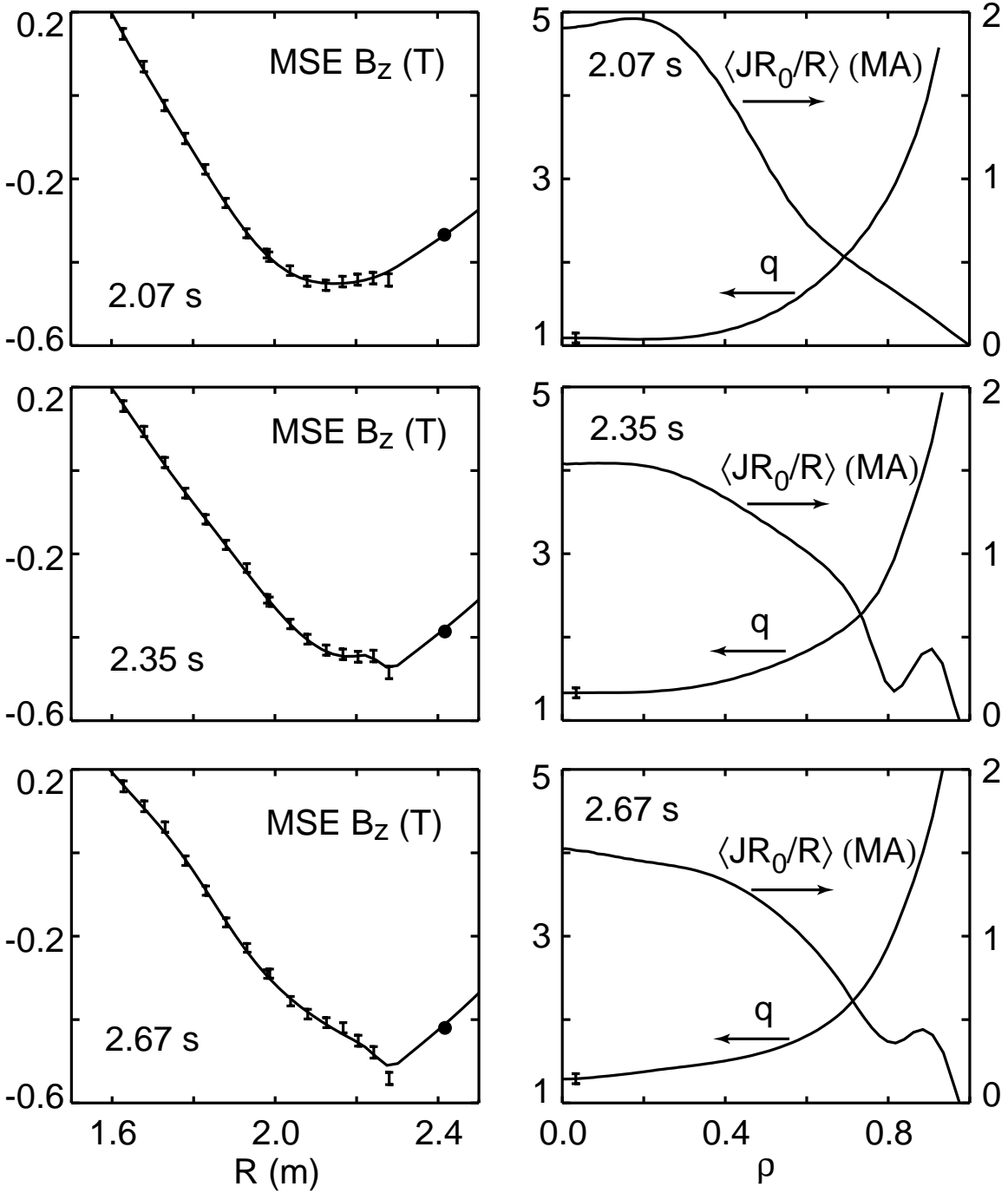


FIG. 7. Current profile evolution for VH-mode discharge 83710, showing increasing q_0 and the development of edge current.

C. Negative central magnetic shear

A significant increase in performance on DIII-D has been observed in discharges with negative central magnetic shear (NCS) (Rice [10], Strait [11]). Although the benefits of this

configuration were predicted some time ago, an aggressive research effort had to be delayed until a reliable and routine measurement of the q profile was available. Thus, the MSE diagnostic has played a key role in initiating this area of research.

NCS discharges are produced on DIII-D using 5 MW of neutral beam injection early in the initial current ramp. As the beam power is increased (in the range 7–15 MW), a transport barrier is observed to develop near the radius of q_{\min} , for the ion temperature T_i and toroidal rotation f_ϕ , and in some cases density and electron temperature as well. Profiles of poloidal field, q , toroidal rotation, and ion temperature are shown for one typical high performance negative shear discharge in Fig. 8. The reduction in the gradient of the poloidal field near the magnetic axis is clearly seen in the MSE data, corresponding to low on-axis current density and high q_0 . The steep gradient in f_ϕ and T_i is localized near the radius of q_{\min} , indicating the presence of a local transport barrier. Given the success of these experiments, we are continuing a program on DIII-D to further optimize the NCS configuration.

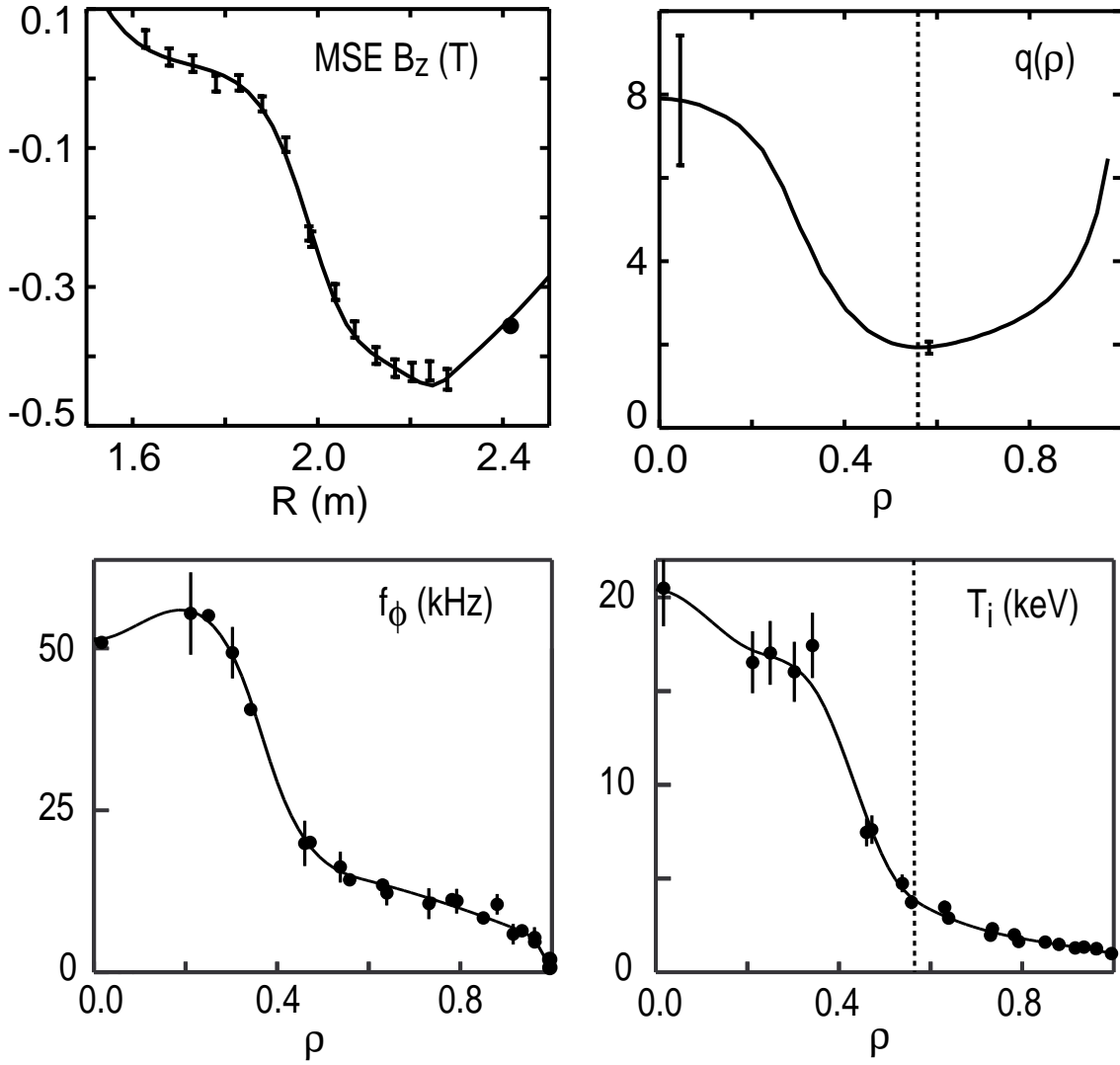


FIG. 8. Negative central magnetic shear profiles produced with early neutral beam injection. A transport barrier in T_i and f_ϕ is observed near the radius of q_{\min} .

6. CONCLUSION

A 16-channel MSE diagnostic is used to obtain local measurements of the poloidal field and $q(r)$ on DIII-D. Recent upgrades in the design have increased the number of channels, and improved the spatial resolution and calibration, leading to a more reliable and routinely used instrument. Coupled with the EFIT equilibrium reconstruction code, rapid profile analysis is now possible in the control room between discharges. Access to fast and accurate q profile measurements has improved our understanding of plasma stability and confinement in advanced tokamak operating modes, and has already led to enhanced tokamak performance.

REFERENCES

- [1] F.M. Levinton, *et al.*, Magnetic field pitch-angle measurements in the PBX-M tokamak using the motional Stark effect, *Phys. Rev. Lett.* **63** (1989) 2060–2063.
- [2] D. Wroblewski, *et al.*, Motional Stark effect polarimetry for a current profile diagnostic in DIII-D, *Rev. Sci. Instrum.* **61** (1990) 3552–3556.
- [3] D. Wroblewski and L.L. Lao, Polarimetry of motional Stark effect and determination of current profiles in DIII-D, *Rev. Sci. Instrum.* **63** (1992) 5140–5147.
- [4] B.W. Rice, D.G. Nilson, and D. Wroblewski, Motional Stark effect upgrades on DIII-D, *Rev. Sci. Instrum.* **66** (1995) 373–375.
- [5] Reflector manufactured by Optical Coating Laboratory Inc., Santa Rosa, California.
- [6] L.L. Lao, *et al.*, *Nucl. Fusion* **30** (1990) 1035.
- [7] D. Wroblewski and R.T. Snider, *Phys. Rev. Lett.* **71** (1993) 859.
- [8] J.R. Ferron, *Rev. Sci. Instrum.* **63** (1992) 5414.
- [9] E.A. Lazarus, *et al.*, The role of shaping in achieving high performance in DIII-D, *Plasma Phys. and Contr. Nucl. Fusion Research, 1994* (International Atomic Energy Association, Vienna, 1995) to appear.
- [10] B.W. Rice, *et al.*, Demonstration of high performance negative central magnetic shear discharges in the DIII-D tokamak, *Phys. Plasmas*, to appear.
- [11] E.J. Strait, *et al.*, *Phys. Rev. Lett.* **75**, 4421 (1995) .

ACKNOWLEDGMENT

This is a report of work supported by the U.S. Department of Energy under Contract Nos. DE-AC03-89ER51114 and W-7405-ENG-48.